Atmospheric Environment 247 (2021) 118193

Contents lists available at ScienceDirect

Atmospheric Environment

journal homepage: http://www.elsevier.com/locate/atmosenv

Wildland fire emission sampling at Fishlake National Forest, Utah using an unmanned aircraft system

J. Aurell [a], B. Gullett [b,*], A. Holder [b], F. Kiros [a], W. Mitchell [b], A. Watts [c], R. Ottmar [d]

[a] University of Dayton Research Institute, 300 College Park, Dayton, OH, 45469, USA
[b] U.S. Environmental Protection Agency, Office of Research and Development, 109 T.W. Alexander Drive Research Triangle Park, NC, 27711, USA
[c] Desert Research Institute, 2215 Raggio Parkway, Reno, NV, 89512, USA
[d] U.S. Forest Service, Pacific Wildland Forest Sciences Laboratory, 400 North 34th Street, Seattle, WA, 98103, USA

HIGHLIGHTS

- An unmanned aircraft system was used to measure air pollutants from a wildland fire.
- The prescribed fire included slash pile burns and crown fires.
- Emission factors were determined for a comprehensive list of gases and particles.
- Emissions typically decreased with increasing combustion efficiency.
- The system enabled unprecedented access to the fire while minimizing risk.

GRAPHICAL ABSTRACT

ARTICLE INFO

Keywords:
Prescribed fire
Wildfire
Emissions
Measurements
Drone
UAS

ABSTRACT

Emissions from a stand replacement prescribed burn were sampled using an unmanned aircraft system (UAS, or "drone") in Fishlake National Forest, Utah, U.S.A. Sixteen flights over three days in June 2019 provided emission factors for a broad range of compounds including carbon monoxide (CO), carbon dioxide (CO_2), nitric oxide (NO), nitrogen dioxide (NO_2), particulate matter < 2.5 μm in diameter ($PM_{2.5}$), volatile organic compounds (VOCs) including carbonyls, black carbon, and elemental/organic carbon. To our knowledge, this is the first UAS-based emission sampling for a fire of this magnitude, including both slash pile and crown fires resulting in wildfire-like conditions. The burns consisted of drip torch ignitions as well as ground-mobile and aerial helicopter ignitions of large stands comprising over 1000 ha, allowing for comparison of same-species emission factors burned under different conditions. The use of a UAS for emission sampling minimizes risk to personnel and equipment, allowing flexibility in sampling location and ensuring capture of representative, fresh smoke constituents. $PM_{2.5}$ emission factors varied 5-fold and, like most pollutants, varied inversely with combustion efficiency resulting in lower emission factors from the slash piles than the crown fires.

* Corresponding author.
E-mail address: gullett.brian@epa.gov (B. Gullett).

https://doi.org/10.1016/j.atmosenv.2021.118193
Received 30 May 2020; Received in revised form 9 December 2020; Accepted 5 January 2021
Available online 9 January 2021

1. Introduction

Wildland fires, including both prescribed burns and wildfires, are the largest single U.S. source of particulate matter of median diameter 2.5 μm ($PM_{2.5}$ mass median diameter), contributing to cardiopulmonary health issues (Rappold et al., 2017; Kim et al., 2018), and visibility hazards (Hyde et al., 2017). Emissions of $PM_{2.5}$ and precursors to ozone (O_3) formation (nitrogen oxides (NO_X) and volatile organic compounds (VOC)) from wildfires can be a factor in planning strategies to ensure compliance with National Ambient Air Quality Standards. Sampling $PM_{2.5}$ and other air pollutants in the smoke from wildland fires is necessary to determine emission factors for use in dispersion and atmospheric models (Liu et al., 2019). These models can be used to predict air quality effects and health risks which are factors in policy and management decisions. Emission factors have been determined for a broad array of biomass types and geographies over the last few decades (Prichard et al., 2020). Advances in instrumentation and requirements for greater speciation detail and temporal data have promoted refinement of these measurement methods.

Obtaining representative samples from open fire sources without undue risk to personnel and equipment poses considerable challenges. Ground-based collection of samples can result in a biased sample representing only the more safely-sampled smoldering, rather than flaming, portion of the emissions, both of which have considerable differences in emission production (Hsieh et al., 2018). Ground-mobile approaches may have rectified this concern somewhat (Alves et al., 2011a, 2011b; Vasileva et al., 2017). Other approaches to wildland fire emissions quantification have included laboratory burns (Gilman et al., 2015; Selimovic et al., 2018; Jen et al., 2019) and studies that combine or compare laboratory-, ground-, and aircraft-based measurements (Ward and Radke, 1993; Simpson et al., 2011; Akagi et al., 2013; Yokelson et al., 2013; Weise et al., 2015; Liu et al., 2017; Hodshire et al., 2019). Many of these studies examine emissions as a function of modified combustion efficiency (MCE = carbon dioxide (CO_2)/(carbon monoxide (CO) + CO_2) which may tie these disparate sampling methods together and minimize potential bias (Urbanski, 2013; Yokelson et al., 2013).

In recent years the advent of unmanned aircraft systems (UAS, or "drones"), specifically multicopter UAS, along with low-cost, miniature sensors, have provided another solution toward the sampling issues of risk, representativeness, and cost. UAS-based emission sampling systems have been demonstrated on demilitarization plumes (Aurell et al., 2017b; Zhou et al., 2017), prescribed forest fires (Nelson et al., 2019), and open industry flares (Krause and Leirvik, 2018) presenting an alternative solution to the challenges in characterizing wildland fire emissions. The principle disadvantage of UAS sampling is the payload weight limitation for the instrumentation and the limited battery life. The use of battery operated UAS is critical for emission sampling, to avoid sampling combustion exhaust from the UAS along with the burn emissions. Together, airplane, ground, and UAS sampling systems provide a complementary suite of measurement approaches for characterizing wildland fire emissions.

The unpredictability of wildfire occurrence and the increased hazard to sampling personnel and equipment have limited the number of near-source emission measurements on these large fires. The event timing for prescribed burns are generally predictable, allowing for setup of emission monitoring equipment and other fire-related measurements that have provided a greater number of references. Risks to personnel and equipment are minimized due to the typically low fire intensity. Differences in emission factors from prescribed and wildfires have been observed (Volkova et al., 2014) but have been hard to reconcile due to the lack of wildfire data. Some data indicate that wildfires have PM_1 emission factors twice those from prescribed fires, however, these data in the U.S. are limited in number and location (Liu et al., 2017), with focus on northern and northwestern states (Radke et al., 1991; Friedli et al., 2001; Urbanski, 2013).

To address the data gap for larger wildland fires and to improve operational wildland fire and smoke prediction systems, an interagency effort entitled Fire and Smoke Model Evaluation Experiment (FASMEE) was created and designed to incorporate coordinated field campaign measurements into fire and smoke modeling capabilities (Ottmar et al., 2017; Prichard et al., 2019). In June 2019 the FASMEE project was teamed with the Monroe Mountain Aspen Ecosystems Restoration Project ("Final Environmental", 2015) to sample a prescribed burn at Manning Creek, South Monroe, Utah. The Project encompasses approximately 70,000 ha of national forest system lands on the Richfield Ranger District of the Fishlake National Forest. The purpose of the project is to restore aspen ecosystems through a combination of mechanical harvesting and reintroduction of "natural fire" through use of prescribed burns in a mosaic pattern. These burns are meant to lower hazardous fuel accumulations, reducing the risk to life, property, and natural resources, while promoting aspen regeneration. The Manning Creek burn provided the FASMEE team an opportunity to sample a prescribed fire with heavy surface fuel loads (50–100 Mg/ha) resulting in a high intensity surface and crown fires with dynamic long-range plumes relevant for smoke management (Prichard et al., 2019). Three days of emission sampling resulted in samples from drip-torch-lit slash pile fires and ground mobile terra-torch and heli-torch ignitions of standing forest. The FASMEE project enabled demonstration of UAS-borne sensors and samplers for characterizing emissions from a large wildfire-like crown burn. Emissions were collected from both aerial sampling (n = 15) using a UAS and an opportunistic ground-based sample (n = 1). To our knowledge, UAS-based emission sampling on wildfire-like crown burns has not previously been demonstrated.

2. Experimental

The Fishlake National Forest in Utah is located approximately 37 km south of Richfield, Utah at altitudes ranging from approximately 2600 m to 2900 m. The area is populated with mixed conifers (spruce, fir, ponderosa pine (*Pinus ponderosa)*), quaking aspen (*Populus tremuloides*), sagebrush with grasses, forbs (grazed annually) along with cut/cured and piled activity fuels ("South Monroe", 2019). Mixed conifers show insect and disease damage. The site has been targeted for a planned stand replacement effort as part of the Restoration Project. Fuel loadings range from 45 to 370 Mg/ha ("South Monroe", 2019). The Manning Creek area of the Forest, where the study occurred, comprised 770 ha with a measured pre-burn loading of 56–134 Mg/ha (Freeborn et al., 2015) and an estimated post-burn consumption of 49 Mg/ha. Future efforts by other teams are expected to determine consumption through use of the fuel characteristic classification system using collected data collected and exercise of the CONSUME program (Ottmar, 2013).

Hand drip-torch, ground-mobile torch, and heli-torch ignitions were conducted, the latter to favor a free-running uphill fire. Three different burn scenarios were conducted on consecutive days, from June18–20, 2019. Day one was on a 12–18 month old slash pile burn (hereafter "Slash") consisting of piled, mixed conifers (Engelman spruce (*Picea engelmannii*), subalpine fir (*Abies lasiocarpa*), and white fir (*Abies concolor*)) and minor amounts of aspen present. Minimal live moisture was present but the area had seen recent melting from a 200% above normal snow pack. The single pile size was about 10 × 20 × 2 m high and was hand lit by drip torch. Day two consisted of "knob" burns (hereafter "Knob") which were two forested areas totaling about 35 ha protruding about 25 m above the surroundings. The Knob units had been thinned, leaving primarily aspen and some slash on the ground. The Knob burns were lit by ground-mobile torch and consisted of ground and crown fires. The day three scenario was the largest burn, about 700 ha, ignited by heli-torch over a 2–3 h period, which consumed the whole stand through a crown fire (hence, "Crown"). The Crown unit contained mixed conifer standing trees with patches of aspen.

Emission sampling took place centered at 38°, 26′, 31.08″ N and 112°, 3', 40.69″ W on an area called "Big Flat Reservoir". The Knob and Crown fires were detected by the National Oceanic and Atmospheric

Administration (NOAA) and Suomi National Polar-orbiting Partnership (NPP) satellites using the Visible Infrared Imaging Radiometer Suite (VIIRS). Estimates of fire radiative power (FRP) from the Hazard Mapping System (HMS) dataset resulted an FRP ranging from 6 to 16 MW (MW) for the Knob burns about 1 h into the 3 h sampling period. These values declined to a maximum of 2.1 MW after midnight on the 19th reflecting continued smoldering. The Crown fire on June 20, 2019 resulted in a high intensity, ground and crown fire with a maximum FRP of 269 MW (and a low of 15 MW) recorded several hours after initiating heli-torch ignitions and less than an hour prior to UAS/Kolibri emission measurements.

Gas and particle sampling were accomplished using the "Kolibri", a battery-powered, remotely controlled instrument comprised of sensors and samplers for an array of pollutants listed in Table 1. The shoe-box-sized Kolibri weighs approximately 3.2 kg and has dimensions of 17 × 17 × 32 cm. The unit is self-powered with a lithium polymer battery and was attached to the undercarriage of the UAS. A USB-based microcontroller board (Teensy 3.2, PJRC, LLC., Sherwood, OR, USA) runs the Arduino-based data acquisition, voltage regulation system, and on-board control program. The Kolibri operator uses a ground-based computer to run a Labview generated data acquisition and control program, providing live data and run/control via a XBee wireless network (Xbee S1B, Digi International, Inc., Minnetonka, MN, USA). The Kolibri reports real time sensor-measured gas concentrations to the operator to better optimize sampling position of the UAS. The main components of the Kolibri are described briefly below and additional descriptions of the system can be found in the literature (Aurell et al., 2017b).

The Kolibri consists of electrochemical and infrared sensors as well as sample collection media. All sensors were selected for their applicability to the expected concentrations and ambient conditions, their ability to respond rapidly to fluctuations in concentrations, and their lack of interference from other gases. Sensor performance was evaluated in the laboratory and calibration curves were obtained prior to field deployment. Evaluations included sensor performance (detection limits, linearity, drift, response time, noise) in response to anticipated field temperatures, pressure, humidity, and interferences (covered in part in Aurell et al., 2017b; Zhou et al., 2017).

The CO_2 sensor (CO_2 Engine® K30 Fast Response (FR), SenseAir, Delsbo, Sweden) measures CO_2 concentration by means of non-dispersive infrared absorption (NDIR). The CO_2 sensor has a measured time to reach 95% of a reference concentration, t_{95}, at 6000 ppm CO_2 of 9.0 ± 0.0 s with a noise level of 1.6 ppm. The response time was 4 s longer than compared to CO_2 measured by a portable gas analyzer (LI-820, LI-COR Biosciences, Lincoln, NE, USA). The sensor and the LI-820 showed good agreement as the measurements showed a R^2 of 0.99 and a slope of 1.01 (Gullett et al., 2020).

Table 1
Sampled emissions and measurement methods.

Analyte	Instrument/Method	Frequency
CO_2	NDIR	Continuous, 1 hz
CO	Electrochemical cell	Continuous, 1 hz
$PM_{2.5}$	Impactor/Teflon filter/ gravimetric	Batch
Elements	X-ray fluorescence (XRF)	Batch
VOCs	Carbotrap® 300	Batch
Carbonyls	DNPH cartridge	Batch
Black carbon	Micro Aethalometer, MA200/350	Continuous, 1 hz
Elemental carbon/Organic carbon/ Total Carbon (EC/OC/TC)	Quartz filter	Batch
NO_2	Electrochemical cell	Continuous, 1 hz
NO	Electrochemical cell	Continuous, 1 hz

The CO sensor (EC4-500-CO) is an electrochemical gas sensor (SGX Sensortech, Essex, United Kingdom) which measures CO concentration by means of an electrochemical cell through CO oxidation and changing impedance. The sensor was compared (Zhou et al., 2017) with simultaneous measurements by a CO continuous emission monitor (CEM, CAI Model 200, California Analytical Instruments Inc., Orange, CA, USA) with laboratory biomass burns. The two concentration measurements had an R^2 of 0.98 and a slope of 1.04, indicating a good comparison. The t_{90} of the sensor was 18 s; comparison with the CAI-200 which had a manufacturer's t_{90} of <1 s, indicated only a 4.9% difference in the time-integrated CO concentration (Gullett et al., 2020).

The nitric oxide (NO) sensor (NO-D4) and the nitrogen dioxide (NO_2) sensor (NO2-D4) are also electrochemical cells (Alphasense, Essex, United Kingdom). Both sensors measure via changes in impedance. The NO sensor manufacturer rates the NO-D4 at a resolution of <0.1 RMS noise (ppm equivalent) and linearity within ±1.5 ppm error at full scale in a detection range of 0–100 ppm. The NO-D4 was tested to have a response time to t_{95} of 6.3 ± 0.52 s and a noise level of 0.027 ppm. The NO_2 sensor has a t_{95} value measured as 32.3 ± 3.8 s. Its noise level is 0.015 ppm, has a working range of 0–10 ppm with resolution of 0.1 RMS noise (ppm equivalent), and a linearity error of 0–0.6 ppm at full scale (Gullett et al., 2020).

Pre- and post-measurement calibrations on sensors and pumps were conducted on burn days. The pre-measurement calibrations allowed for coefficient adjustments in the calibration curves to account for ambient temperatures and pressures at the measurement site conditions. Post-measurement calibrations allowed for determination of sensor drift. Drift values for mid-concentration values on the sensor calibrations were less than 2% for CO_2, 8% for NO_2, and 1% for NO. The CO sensor drift recorded values of 47% and 12% for two days, the high value suspected to be due to an ill-fitting tube on the calibration gas bottle or sensor inlet.

VOCs were sampled using a Carbotrap® 300 stainless steel Thermal Desorption (TD) Tube (Supelco Inc., Bellefonte, PA, USA) via a constant micro air pump (3A120CNSN, Sensidyne, LP, St. Petersburg, FL, USA) in accordance with U.S. EPA Method TO-17 (1997) and analyzed by TD-gas chromatography/mass spectrometry (GC/MS). Carbonyls were sampled with 2,4-Dinitrophenylhydrazine (DNPH) coated silica cartridges via a constant micro air pump (C120CNSN, Sensidyne, LP, St. Petersburg, FL, USA) and analyzed by high-pressure liquid chromatography using U.S. EPA Method TO-11A (1999a).

$PM_{2.5}$ was sampled with SKC personal environmental monitor impactors using 37 mm tared Teflon™ filter with a pore size of 2.0 μm and a constant micro air pump (C120CNSN, Sensidyne, LP, St. Petersburg, FL, USA) at 10 L/min. Particles larger than 2.5 μm in the $PM_{2.5}$ impactor were collected on a greased impaction disc mounted on the top of the filter. $PM_{2.5}$ mass was measured gravimetrically following the procedures described in 40 CFR Part 50 Appendix J and L (1987a; 1987b). Potential effects of rotor wash on particle measurements are a common and open question. Laboratory burn tests with and without a fan-simulated rotor wash (Zhou et al., 2017) showed only a 4% difference in the $PM_{2.5}$ emission factors and an R^2 value of 0.95 when comparing the time-resolved $PM_{2.5}$ measurements. These comparisons lend confidence to the methods employed here, yet additional verification would be desirable. Metal/element species were determined by x-ray fluorescence spectrometry (XRF) analysis of the Teflon $PM_{2.5}$ filters using EPA Compendium Method I0-3.3 (1999b).

Black carbon (BC) was measured with an AE51 and MA200 micro-aethalometer (AethLabs, U.S.A.) which are small, portable, hand-held instruments. The AE51 and MA200 measure BC concentration using a calibrated filter-based light attenuation measurement at 880 nm, which is the same operating principle for all aethalometers. Additionally, the MA200 measures light attenuation at four other wavelengths in the ultraviolet and visible range (625, 528, 470, and 375 nm) on two spots simultaneously to allow for filter loading correction (Drinovec et al., 2015). The variation in absorption by wavelength is quantified by the absorption Ångström exponent (AAE), which is calculated from the

MA200 data by fitting a linear regression of the form:

$$\ln(BC_\lambda) = (1 - AAE)\ln(\lambda) + const$$

where BC_λ represents the measured absorption coefficient at wavelength λ. Light absorbing carbon, i.e. brown carbon, is sometimes quantified as Ultra violet PM (UVPM), which is the equivalent mass of BC that would result in the excess absorption at 375 nm (Hansen, 2005). The MA200 contains 15 sampling locations on an automatic filter tape advance system, allowing for long-term near-continuous measurements without the need for repeated filter replacements necessary for the AE51.

Organic/Elemental/Total Carbon, OC/EC/TC, was sampled with an SKC (Eighty Four, PA, USA) $PM_{2.5}$ personal modular impactor using a 37 mm quartz filter via a constant micro air pump (C120CNSN, Sensidyne, LP, St. Petersburg, FL, USA) of 3 L/min. An oiled 25 mm impaction disc mounted on the top of the filter cassette collected particles larger than 2.5 μm. The OC/EC/TC was analyzed using a modified thermal-optical analysis using Modified NIOSH Method 5040 (1999c) and Khan et al. (2012). All constant flow pumps were calibrated daily with a Sensidyne Go-Cal Air Flow calibrator. The Kolibri is also equipped with a global position system (GPS) sensor (Ultimate GPS Breakout V3) and a temperature and barometric pressure sensor (BMP 180, both from Adafruit, New York, USA).

The Kolibri was affixed to the fuselage of a DJI M600 Pro UAS (Fig. 1). The M600 is a six motor hexacopter which was equipped with specialized rotors for high altitude flight. The aircraft were manually piloted with assistance from ground-based visual observers and aircraft-mounted cameras, allowing the sampling payload to be positioned accurately in order to achieve precision sampling of smoke plumes. Telemetry of onboard temperature measurements permitted the aircraft and payload to maneuver at distances from fires without placing the system in temperatures that would cause damage to components. Real-time CO_2 sensor readings assisted the pilot in remaining within a desired portion of the smoke plume for the duration of sampling. Wind and turbulence around plumes affected flight duration of the battery-powered aircraft, but sampling flights ranged in duration from five to 13 min.

Emission factors, or the mass of pollutant emitted per mass of fuel burned, were determined using the carbon balance method (adopted from Ward et al., 1979; Ward and Hao, 1991; Laursen et al., 1992):

$$EF_i = f_c \times \frac{Analyte_{ij}}{C_j}$$

where:

EF_i = Emission Factor for target analyte i (mass analyte i/$mass_{biomass}$ burned).

f_c = mass fraction of carbon in the biomass.

$Analyte_{ij}$ = background-corrected concentration (mass analyte i/volume) of the target analyte i collected from the volume element j of the plume.

Cj = background-corrected concentration of carbon (mass C/volume) collected from volume element j of the plume, based on CO, CO_2, and carbon in the particulate matter. The latter is determined by a TC analysis from the simultaneously sampled quartz filter.

This ratio is multiplied by the carbon fraction in the biomass, f_c, which requires foreknowledge or assumption of the fuel's carbon composition, in this case assumed at 50%. Mixed conifer types abound at the burn area's higher elevations, consisting of older age class Engelmann spruce or Douglas-fir trees intermixed with aspen, white fir, subalpine fir, and mountain shrub. This species mix makes calculation of a representative carbon fraction problematic. We use an approximate carbon fraction value of 0.50 or 50%, reflective of values in Williams et al. (2017) (0.507, woody, Table 1) and Thomas and Martin (2012) (0.508, temperate, boreal conifer, Table 2).

Upon combustion, the volatilized fuel carbon is presumed to proceed to CO_2, CO, and particulate carbon, with the minor mass of carbon in emitted VOCs often ignored as having little influence on the calculation. To compensate for the rapid, turbulent dilution of the plume which results in gas concentration fluctuations of shorter order than the sensors' t_{90} values, time-integrated values of the sampled gases are used in all emission factor calculations. Concurrent measurements of the pollutant mass and carbon mass multiplied by the carbon fraction in the fuel results in the emission factor, or pollutant mass per fuel mass consumed. Similar methods were employed for all pollutants, whether gaseous or particulate. All reported emission factors were corrected for background concentrations of pollutants determine by extended sampling of local, ambient, smoke-free air.

Fig. 1. Kolibri attached to the undercarriage of the UAS.

3. Results

3.1. Test results

A total of 16 UAS-based samples plus one ground-based sample and one ambient air background sample were taken over a 3-day period from June 18 to June 20, 2019 encompassing slash pile burns, elevated "knob" burns amounting to about 35 ha total area, and a large crown/stand replacement burn (Fig. 2) comprising over 750 ha. The UAS/Kolibri operational locations and the three burn areas are located on Fig. 3. $PM_{2.5}$, NO_x, and metals were measured/sampled every flight while EC/OC/TC, BC, VOC, and carbonyls were traded off due to payload limitations. The UAS was maneuvered into a hovering position in the plume with the aid of both real time CO_2 data, indicating its presence within the combustion gases, and a gimbal-mounted visual camera providing real time video of the smoke. Maximum UAS above ground level altitude ranges and sampling (not flight) durations for the Slash piles, Knob burns, and Crown burns were, respectively, 25 m–133 m (79 m average) and 8 min, 31 m–151 m (81 m average) and 9 min, and 224 m (6 min) (the GPS data transmission failed on the second flight). The average flight duration was 15 min after which the UAS returned for battery replacement and changes in filters, VOC tubes, and carbonyl tubes. The effective sampling period, less transit time to and from the plume, ranged from 5 to 13 min. The Slash and Knob burns were sampled for over 2 h duration. The Crown burn sampling commenced after the heli-torch landed and flight durations totaling about 20 min were compiled until flight operations ceased. The highest elevation of the UAS during the Crown burn was about 224 m above the UAS take off/landing area. The order of these sources enabled the sampling team and pilots to gain experience with increasing fire intensity. The changes in fire intensity allowed examination of fire dynamics and combustion efficiency effects on emission factors.

3.2. Particle results

Particle-based emission factors are summarized Table 2. The 17-sample $PM_{2.5}$ emission factor is 15.1 g/kg biomass with a sample-weighted,

Table 2
Summary particle emission factors.

	Slash Pile			Knob Burn			Crown Burn			Crown Burn			Crown Burn	All Burns
	UAS			UAS			UAS and Ground			UAS			Ground	Run Avg'd
Pollutant g/kg biomass	N	Avg.	RSD, RPD %	n	Avg.	RSD, RPD %	n	Avg.	RSD, RPD %	n	Avg.	RPD%	n	EF	EF
$PM_{2.5}$	5	7.5	23.5	9	18.0	21.9	3	19.1	13.4	2	18.9	26.8	1	19.5	15.1
EC	2	0.1	5.0	6	0.3	52.5	3	0.3	53.7	2	0.4	39.9	1	0.1	0.3
OC	2	7.9	1.8	6	14.9	16.6	3	18.8	14.3	2	18.3	27.8	1	19.8	14.7
TC	2	8.0	1.9	6	15.2	16.4	3	19.1	14.3	2	18.7	28.3	1	19.9	15.0
BC		NS		1	1.88		3	1.02	41	2	1.0	85.2	1	1.1	1.1
UVPM		NS		1	5.29		1	6.9			NS		1	6.9	6.1
mg/kg biomass															
P	4	1.2	45	9	4.9	87	3	10.6	66	2	7.2	174	1	17.4	5.0
S	4	43.8	4	9	47.5	92	3	27.5	27	2	27.6	66	1	27.3	42.8
Cl	4	36.5	16	9	40.1	89	3	19.3	45	2	22.3	82	1	13.3	35.3
K	4	206.7	7	9	213.1	83	3	172.8	42	2	148.9	105	1	220.6	204.0
Ca	4	21.6	23	9	67.6	40	3	243.3	72	2	137.8	160	1	454.2	89.1
Mn	4	1.0	27	9	3.2	78	3	7.0	64	2	5.2	175	1	10.6	3.4
Fe	4	0.3	74	9	1.0	54	3	18.3	103	2	5.2	154	1	44.5	4.1
Zn	4	3.0	19	9	3.7	75	3	2.6	48	2	1.8	76	1	4.2	3.3
Br	4	0.3	22	8	0.7	65	3	0.2	30	2	0.2	62	1	0.3	0.5
Sr	4	0.1	49	9	0.5	57	2	2.9	89	1	1.6		1	4.2	0.7

Relative percent differenced (RPD) calculated when n = 2, relative standard deviation (RSD) calculated when n ≥ 3.

Fig. 2. Crown fire at Fishlake National Forest. Photo by. R. Ottmar.

relative standard deviation of <21%. Uncertainty in the $PM_{2.5}$ emission factor values may be driven by the carbon sampling calculations, which are dominated by the major carbon source, CO_2, rather than filter weights, CO, TC, or f_c. This emission factor compares well with a value of 14.32 g/kg biomass compiled from 24 measurements in western pine and mixed conifer forests (Prichard et al., 2020). The $PM_{2.5}$ is primarily comprised of OC at 14.7 g/kg biomass (96 ± 9%), with the balance being EC (2 ± 1%) and other elements (2 ± 1%).

The average $PM_{2.5}$ emission factors for the Slash pile, Knob burns, and Crown burn increase from 7.5 g/kg biomass to 18 g/kg biomass to 19 g/kg biomass, respectively, a 2- to 3-fold increase for similar biomass species, growth environment, and sampling period meteorological conditions. The range of the data covers a 5-fold difference in $PM_{2.5}$ emissions. The average Slash pile $PM_{2.5}$ emission factor compares to previous work sampling wet slash pile burns in the US Northwest of 18 g/kg and dry slash piles that ranged from 3.4 to 6 g/kg (Aurell et al., 2017a). Single factor analysis of variance (ANOVA) found significant differences (p-value< 0.05, F/Fcrit > 1) in $PM_{2.5}$ emission factors between the Slash pile burns and both the Knob burns and Crown burns.

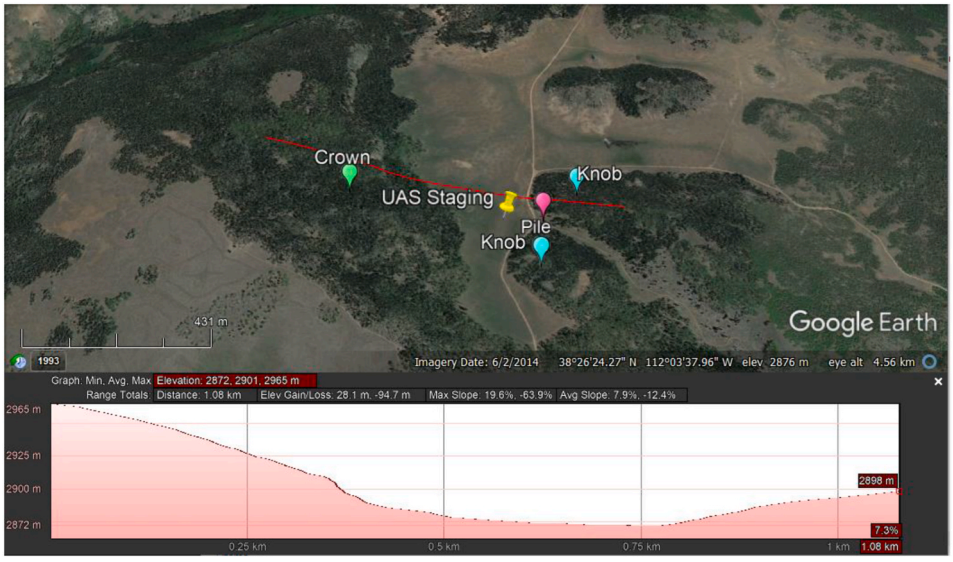

Fig. 3. Google Earth image of UAS/Kolibri flight area locations in the Big Flat Reservoir area of Fishlake National Forest, Utah. Red path line shows the elevation contour in the inset. (For interpretation of the references to color in this figure legend, the reader is referred to the Web version of this article.)

The Knob burns and Crown burns failed to meet the significance criteria (p-value< 0.05, $F/F_{crit} > 1$) for distinction. The relatively high density of the Slash pile biomass and the minimal live tree moisture (the estimated age of the piles was 12–18 months) would both have contributed to higher temperatures and improved combustion. The piles would also have been subjected to the greatest potential constraint on oxygen diffusion to the pile center compared to the open Knob and Crown burns and likely would have had the longest duration of smoldering. Note that the duration of active pile emission sampling lasted only for 3 h and did not capture the bulk of residual smoldering throughout the evening.

The effect of combustion conditions is examined in Fig. 4 which shows the $PM_{2.5}$ emission factor plotted against the gas phase modified combustion efficiency, MCE_g. The emission factor and combustion efficiency relationship described thoroughly by Urbanski (2013) shows that for any one fire type (Slash, Knob, Crown) the emissions are linearly related to combustion quality. For high PM-emitting burns, inclusion of the particulate carbon in the combustion efficiency calculation, MCE_T, should be considered. Payload limitations on the UAS, however, limited the number of particulate carbon samples that could be taken throughout the 3-day period as this sampler was periodically traded off for different sample media. As such, fewer MCE_T values (Fig. 5) are available than the MCE_g values.

The elemental speciation is dominated by potassium (K) and calcium (Ca), comprising 85% of the ten elements listed. These elements are followed by sulfur (S) and chlorine (Cl) in about a 1:1 ratio comprising 10% of the ten-element mass. The ten elements listed in Table 2 amount to just under 800 mg/kg, or about 5% of the particle mass (Table 3), which is typical for most biomass burning emissions (Jaffe et al., 2020). The highest elemental particle mass percentages were seen from the first Slash pile burn sample and the ground sample of the Crown burn. This Crown sample was the only sample with elevated crustal elements (magnesium (Mg), aluminum (Al), silicon (Si), and iron (Fe)), which suggests that some soil may be entrained at ground level but not lofted in the plume. The Slash pile sample was enriched with phosphorus (P), S, Cl, and K, and this was also the sample with the highest average MCE_g and MCE_T values. This varying inorganic composition may be due to varying fuel composition and combustion conditions, as some shrubs and grasses and flaming-dominated samples have larger inorganic $PM_{2.5}$ percentages (Ward and Hardy, 1988; Levin et al., 2010). The full list of elements is in Supporting Information (SI) Table S-1.

The sum of the OC and all measured elements is approximately 100 $\pm$ 2% of the $PM_{2.5}$ mass measured on the Teflon filters. Lighter weight elements, like oxygen (O) and nitrogen (N), are not measured and may contribute substantially to the $PM_{2.5}$ mass. The OC contribution may also be biased high due to gas phase OC absorption onto the quartz filters (Subramanian et al., 2004).

Linear regressions on the elemental emission factors comparing the Slash, Knob, and Crown burns show little statistical distinction until the single ground-based Crown sample is included in the consideration. Increases in the crustal elements (e.g., Ca and Fe), make the three-sample Crown values distinctive from the slash values ($R^2 = 0.31$, $p = 0.10$) but not the Knob values. Inclusion of the Crown burn ground-based collector results may highlight emission distinctions with the aerial samples, but the limited sample size tempers any such conclusions.

Five BC measurements were made: two Knob burns and three Crown burns (two from the air and one from the ground) ranging from 0.43 to 1.88 g BC/kg biomass. The Knob burns averaged 1.16 and the Crown burns averaged 1.02 g BC/kg biomass. The BC emission factor of 1.1 g/kg is twice the Oregon value of 0.47 g/kg and the average value of 0.55 g/kg for temperate forests compiled by Andreae (2019). The BC emission factors were over three times greater than the EC emission factor for the Knob and Crown burns, but the comparison is limited by few BC samples and differing sample times. BC and EC measurements from biomass burning frequently disagree, with some reporting moderately larger BC emissions than EC emissions (~1.7 times) (Aurell et al., 2015, 2017a) and others reporting lower BC emissions compared to EC (0.8–1.1 times) (Li et al., 2019). These differences can be due to instrument artifacts caused by excessive filter loading of light attenuation-based instruments as well as from variations in the optical properties of the particles. Li et al. (2019) observed larger disagreement among measurement methods with biomass burning emissions that had higher AAEs and more light absorbing OC.

The overall BC and UVPM values (Table 2) reflect the light absorbing OC dominance, at 1.1 and 6.1 g/kg biomass, respectively. This contrasts with pile burns in Oregon where both the BC and UVPM were approximately the same and up to an order of magnitude lower (0.24–0.5 g/kg biomass). Different instruments were used in each study and the AE52 used in Oregon was not corrected for a filter loading artifact unlike the MA200 used here. The UVPM value may have been artificially reduced due to the loading artifact, which may be why the AAE of the Oregon pile burns was approximately 1, which is characteristic of PM with a high EC fraction (~50% or greater) (Bond and Bergstrom, 2006). Most biomass burning emissions have AAEs greater than 1.5 (Holder et al., 2016; Li et al., 2019) to as high as ~3.5 for the Rim wildfire in California (Forrister et al., 2015). This wide range is due in part to the varying

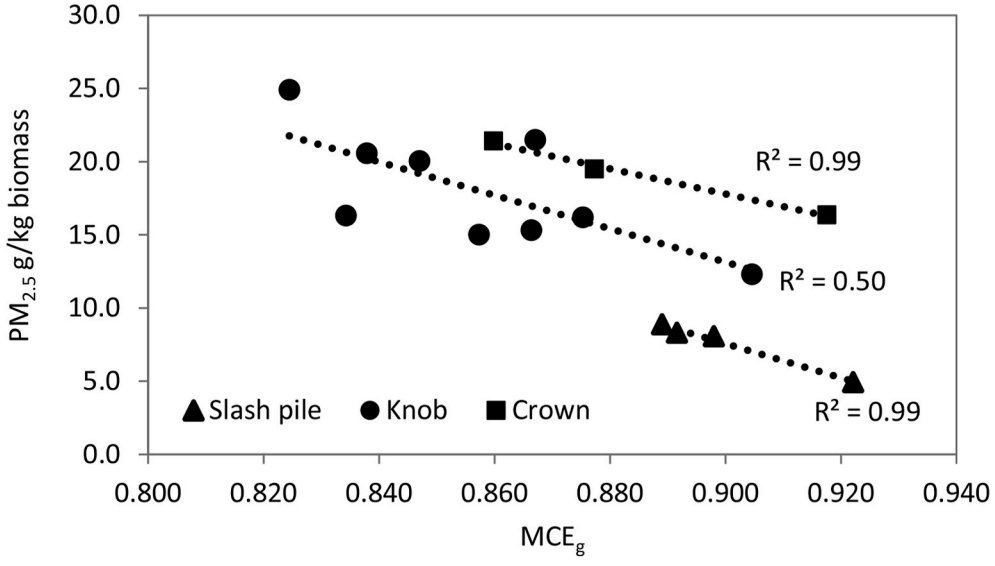

Fig. 4. The effect of gas phase modified combustion efficiency on the $PM_{2.5}$ emission factor for all three burn sources.

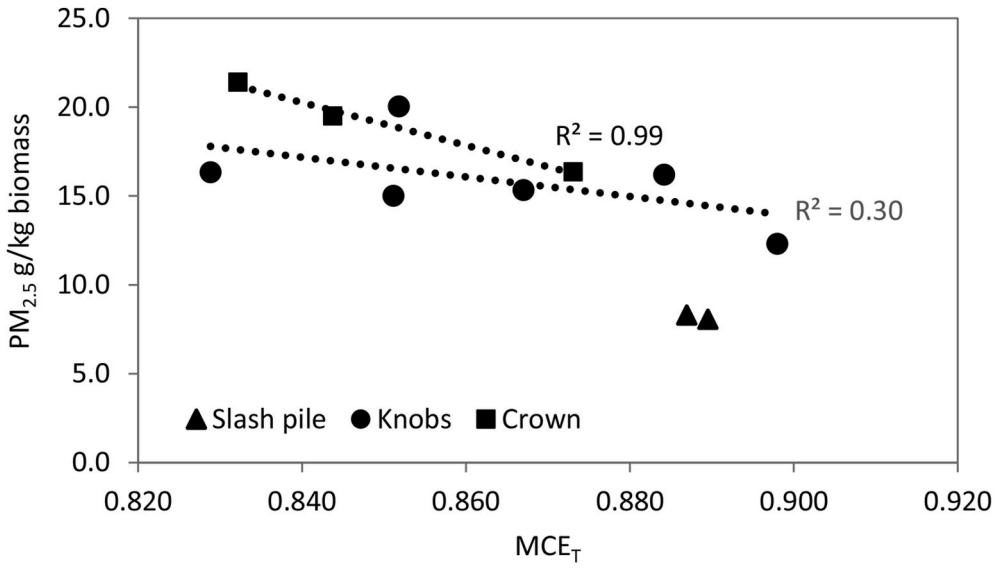

Fig. 5. The effect of modified combustion efficiency calculated with particulate carbon (MCE_T) on the $PM_{2.5}$ emission factor for all three burn sources.

Table 3
Particle composition and optical properties.

	Slash Pile			Knob Burn			Crown Burn		
	UAS			UAS			UAS		
PM Composition %	n	Avg.	RSD, RPD %	n	Avg.	RSD, RPD %	n	Avg.	RPD%
MCE_g	2	0.904	0.7	6	0.864	2.8	2	0.889	6.5
MCE_T	2	0.888	0.3	6	0.863	2.9	2	0.853	4.8
OC	2	96.3	1.1	6	94.5	12.6	2	97.0	1.1
EC	2	1.4	2.0	6	2.0	25.6	2	2.1	13.5
Inorganic species	4	4.5	29.2	9	2.0	67.5	2	2.0	104.0
Sum of Species	2	99.2	0.9	6	97.8	11.5	2	101.0	3.7
AAE		NS		1	2.19		1	3.07	

NS = Not Sampled.

combustion conditions since AAE increases with decreasing MCE (Holder et al., 2016). For example, the Knob burn had an AAE of 2.19 at an MCE_g of 0.911 and the Crown burn had an AAE of 3.07 at an MCE_g of 0.882, however AAE could only be calculated for one sample from each burn.

Values of EC/OC/TC similarly increase from Slash pile burns to Knob burns to Crown burns. Previous work (Aurell et al., 2017a) has shown these values to increase when first sampling dry, covered piles and then wet slash piles or from better to worse combustion conditions. Figs. 4 and 5 show that the combustion efficiencies for the Slash burns were higher than the majority of the subsequent Knob and open Crown burns.

3.3. VOC results

Gas phase emissions for the most prevalent VOCs and the subset carbonyls are summarized in Table 4 and Table 5, respectively. Two samples were taken from the Knob burns and one from the ground-based sampled during the Crown burns. The full list of VOCs is in SI Table S-2. The 62 VOCs analyzed totaled over 1.8 g/kg biomass with the highest contributors (acetone, benzene, toluene, acetonitrile, and m,p-xylenes) accounting for 73% of the mass. Emission factors values were generally consistent with previous slash piles burns in Oregon (Aurell et al., 2017a). Values for toluene, acetonitrile, and m,p-xylenes were higher than in the Oregon study (Aurell et al., 2017a) but within a factor of 2 or 3.

The carbonyls consist of one Slash pile sample, three Knob burn samples, and one aerial Crown sample. The 14 carbonyls measured totaled almost 7 g/kg of biomass, with the two most prevalent carbonyls, hexaldehyde and acetaldehyde, comprising over 60% of the carbonyl mass emitted. The aldehydes follow MCE trends consistent with those identified by Urbanski (2013): in general, higher emission factors are observed at lower combustion efficiencies. Aldehydes are important for their contribution to downwind ozone production (Baker et al., 2016).

Table 4
Summary of volatile emission factors.

	Knobs			Crown		Both
Pollutant, mg/kg biomass	Air			Ground		Average
	n	**Avg. EF**	**RPD %**	**n**	**EF**	**EF**
Acetone	2	417	7	1	352	395.47
Benzene	2	406	29	1	348	386.94
Toluene	2	340	21	1	305	328.32
Acetonitrile	2	202	120	1	35	146.68
m,p-Xylenes	2	115	30	1	135	121.84
2-Butanone (MEK)	2	111	76	1	26	82.58
Styrene	2	66	15	1	75	68.97
Naphthalene	2	59.6	31	1	66.5	61.89
1,3-Butadiene	2	49.3	27	1	47	48.39
Ethylbenzene	2	43	23	1	54	46.45
o-Xylene	2	38	28	1	47	40.88
n-Hexane	2	22.5	34	1	34	26.47
1,2,4-Trimethylbenzene	2	23	43	1	28	24.48
n-Heptane	1	16		1	28	21.87
n-Octane	2	17	42	1	24	19.70

Table 5
Carbonyl emission factors.

	Slash Pile		Knob Burn			Crown Burn		All Burns[c]	
	UAS			UAS		UAS		Average	
Pollutant, mg/kg biomass	n	Avg.	n	Avg.	RSD, RPD %	n	Avg.	n	EF
Hexaldehyde	1	ND	3	ND		1	ND	0	ND
Acetaldehyde[a,b]	1	ND	3	1204	44	1	1079	4	1173
Formaldehyde[a,b]	1	ND	2	265	44	1	1790	3	606
Acetone[b]	1	ND	3	445	48	1	845	4	558
2,5-Dimethyl-benzaldehyde	1	ND	2	341	2	1	489	3	391
Isovaleraldehyde	1	ND	1	309		1	ND	1	309
Propionaldehyde	1	ND	2	221	15	1	315	3	253
Acrolein[a]	1	ND	2	168	15	1	206	3	181
m&p-Tolualdehyde	1	ND	2	112	24	1	214	3	146
n-Butyraldehyde	1	37	2	106	81	1	167	4	104
Crotonaldehyde	1	ND	1	68		1	ND	1	68
Benzaldehyde	1	ND	3	ND		1	ND	0	
Valeraldehyde	1	ND	3	ND		1	ND	0	
o-Tolualdehyde	1	ND	3	ND		1	ND	0	

[a] On US EPA's list of hazardous pollutants (HAPS) (2008).
[b] On US EPA's target list of photochemical assessment monitoring stations (PAMS) compounds (2013).
[c] Average of all values greater than ND.

Carbonyl emission factors for each sample collect are in SI Table S-3.

3.4. NO_x results

Emission factors for nitrogen oxides (NO_x) ranged from 1.18 to 4.11 g/kg biomass and are show in Fig. 6. These values are consistent with those from temperate forests (2.51 g/kg) (Akagi et al., 2011), mixed conifers (1.41 g/kg) (Prichard et al., 2020) and prescribed fire in the Southeast U.S. (1.31 g/kg) (Akagi et al., 2013), but higher than those cited elsewhere 0.49 g/kg (Liu et al., 2017) for western U.S. wildfires. A single factor ANOVA on the NO_x values confirmed that the Knob burns had a significant difference ($p < 0.036$, $F/F_{crit} = 1.17$ to 3.37) in NO_x emission factors between both the Slash pile burn and Crown burns.

Unlike $PM_{2.5}$ and VOCs, NO_x emission factors do not show a linearly decreasing trend with increasing MCE_g. The Slash pile burn shows higher NO_x values at higher MCE_g. While the relatively low temperatures experienced in these three burn types may make thermal NO_x formation (oxidation of fuel-bound N and combustion of atmospheric N_2 and fuel rich hydrocarbons) unlikely (Mladenovic et al., 2016), the detection of NO_2 only during the Slash pile fires (SI Table S-4) is indicative of higher temperatures and more complete oxidation. The absence of NO_2 from the Knob and Crown fires is at odds with previous results which show emission factor ratios of NO_2/NO greater than 5/1 for western U.S. wildfires (Liu et al., 2017), Southeastern understory prescribed fires (Akagi et al., 2013), and prescribed burns of heavy montane conifer fuels (Burling et al., 2011). These differences can likely be explained by the conversion of NO to NO_2 during plume transport as a function of source to receptor distance, ozone concentration, wind speed

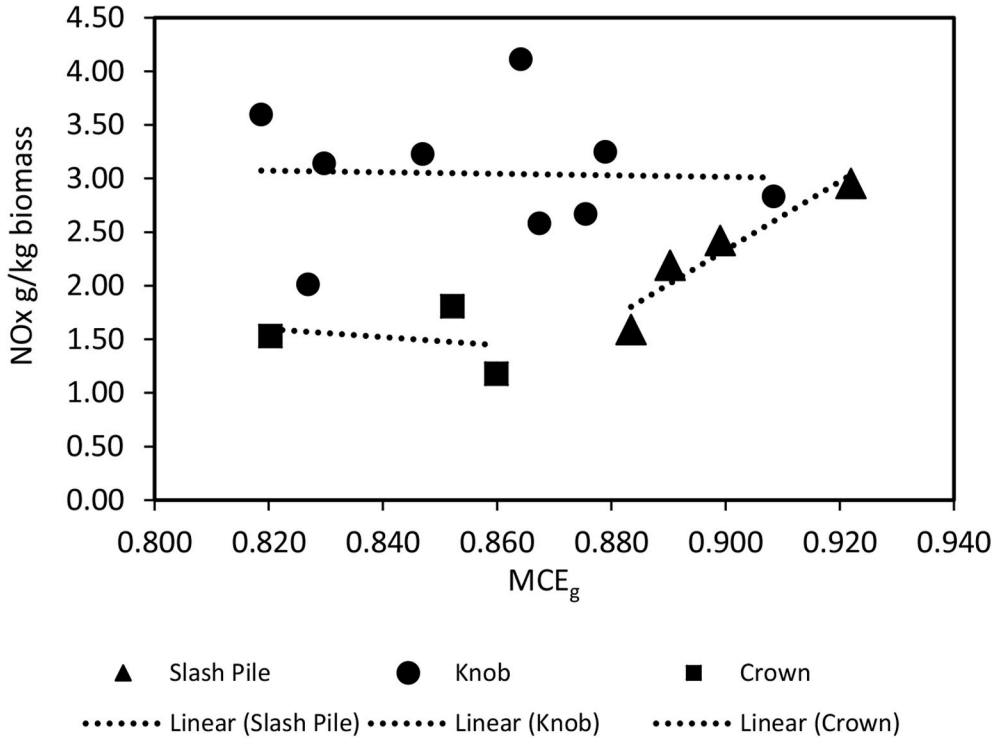

Fig. 6. NO_x species versus MCE_g.

(mixing), and season (Janssen et al., 1988). UAS/Kolibri measurements reported here are closer to the source than the cited airplane or ground-based measurements and are less likely to see NO oxidation. The presence of NO_2 during the Slash Pile burns is likely related to the higher temperatures and MCE values observed compared to the Knob and Crown fires. The NO_2 emission factor for the Slash pile fires (0.94 g/kg biomass) compares with 1.38 g/kg biomass observed for conifer forests (Prichard et al., 2020). NO and NO_2 concentrations in the plumes were low with most peaks reaching 4 ppm and 2 ppm, respectively which was in the lower range of the sensors. For future studies it is recommended to use two NO_2 sensors with different ranges: low (up to 1 ppm) and high (more than 1 ppm) concentrations.

4. Conclusions

The first known sampling of a prescribed fire with wildfire-like crown consumption successfully used a UAS to obtain comprehensive emission data for the determination of emission factors. Results were consistent with the range of published emission factors obtained elsewhere. Distinctions in emission factors were determined between slash piles (lower $PM_{2.5}$, TC, and NO_2) and standing forests comprised of similar species. Emission factors for $PM_{2.5}$ decreased with improved combustion efficiency. The mobility of the UAS-equipped emission sampler enabled adjustment to plume direction changes, improving sampling effectiveness without placing equipment at risk. Operation of the system from a distance further ensured personnel safety.

Declaration of competing interest

The authors declare that they have no known competing financial interests or personal relationships that could have appeared to influence the work reported in this paper.

Acknowledgment and disclaimer

The authors appreciate the analytical assistance of Mike Hays and Ken Krebs, and the FRP analyses of George Pouliot, U.S. EPA. Special thanks to the DRI pilots: Jesse Juchtzer, Dave Vuono, David Page, and Patrick Melarkey. Dave Grimm, Tall Timbers Research Station, coordinated the airspace and team safety. Funding for this work was provided by the U.S. EPA's Office of Research and Development. Author AW acknowledges support from USDA Forest Service Grant # 19-CS-11261987-063, U.S. Joint Fire Science Program Grant # 20-JV-11261987-005, and NASA ROSES Grant # NNX15AI48G. The views expressed in this article are those of the authors and do not necessarily represent the views or policies of the U.S. Environmental Protection Agency.

Appendix A. Supplementary data

Supplementary data to this article can be found online at https://doi.org/10.1016/j.atmosenv.2021.118193.

Data availability

Data used in the writing of this manuscript is available at the U.S. Environmental Protection Agency's Environmental Dataset Gateway (https://edg.epa.gov).

Supporting information

Complete PM elements, VOCs, carbonyl, and NO_x data.

References

40 CFR Part 50, Appendix L, 1987. Reference method for the determination of particulate matter as PM2.5 in the Atmosphere. https://www.gpo.gov/fdsys/pkg/CFR-2014-title40-vol2/pdf/CFR-2014-title40-vol2-part50-appL.pdf. Accessed February, 2019.

40 CRF Part 50, Appendix J, 1987a. Reference method for determination of particulate matter as PM10 in the Atmopshere. https://www.gpo.gov/fdsys/pkg/CFR-2014-title40-vol2/pdf/CFR-2014-title40-vol2-part50-appJ.pdf. Accessed February 13, 2019.

Akagi, S.K., Yokelson, R.J., Wiedinmyer, C., Alvarado, M.J., Reid, J.S., Karl, T., Crounse, J.D., Wennberg, P.O., 2011. Emission factors for open and domestic biomass burning for use in atmospheric models. Atmos. Chem. Phys. 11, 4039–4072.

Akagi, S.K., Yokelson, R.J., Burling, I.R., Meinardi, S., Simpson, I., Blake, D.R., McMeeking, G.R., Sullivan, A., Lee, T., Kreidenweis, S., Urbanski, S., Reardon, J., Griffith, D.W.T., Johnson, T.J., Weise, D.R., 2013. Measurements of reactive trace gases and variable O-3 formation rates in some South Carolina biomass burning plumes. Atmos. Chem. Phys. 13, 1141–1165.

Alves, C., Vicente, A., Nunes, T., Gonçalves, C., Fernandes, A.P., Mirante, F., Tarelho, L., Sánchez de la Campa, A.M., Querol, X., Caseiro, A., Monteiro, C., Evtyugina, M., Pio, C., 2011a. Summer 2009 wildfires in Portugal: emission of trace gases and aerosol composition. Atmos. Environ. 45, 641–649. http://www.sciencedirect.com/science/article/pii/S1352231010009064.

Alves, C.A., Vicente, A., Monteiro, C., Gonçalves, C., Evtyugina, M., Pio, C., 2011b. Emission of trace gases and organic components in smoke particles from a wildfire in a mixed-evergreen forest in Portugal. Sci. Total Environ. 409, 1466–1475. http://www.sciencedirect.com/science/article/pii/S0048969710013562.

Andreae, M.O., 2019. Emission of trace gases and aerosols from biomass burning – an updated assessment. Atmos. Chem. Phys. 19, 8523–8546. https://www.atmos-chem-phys.net/19/8523/2019/.

Aurell, J., Gullett, B.K., Tabor, D., 2015. Emissions from southeastern U.S. Grasslands and pine savannas: comparison of aerial and ground field measurements with laboratory burns. Atmos. Environ. 111, 170–178. http://www.sciencedirect.com/science/article/pii/S1352231015002149.

Aurell, J., Gullett, B.K., Tabor, D., Yonker, N., 2017a. Emissions from prescribed burning of timber slash piles in Oregon. Atmos. Environ. 150, 395–406. http://www.sciencedirect.com/science/article/pii/S1352231016309074.

Aurell, J., Mitchell, W., Chirayath, V., Jonsson, J., Tabor, D., Gullett, B., 2017b. Field determination of multipollutant, open area combustion source emission factors with a hexacopter unmanned aerial vehicle. Atmos. Environ. 166, 433–440.

Baker, K.R., Woody, M.C., Tonnesen, G.S., Hutzell, W., Pye, H.O.T., Beaver, M.R., Pouliot, G., Pierce, T., 2016. Contribution of regional-scale fire events to ozone and PM2.5 air quality estimated by photochemical modeling approaches. Atmos. Environ. 140, 539–554. http://www.sciencedirect.com/science/article/pii/S1352231016304654.

Bond, T.C., Bergstrom, R.W., 2006. Light absorption by carbonaceous particles: an investigative review. Aerosol Sci. Technol. 40, 27–67.

Burling, I.R., Yokelson, R.J., Akagi, S.K., Urbanski, S.P., Wold, C.E., Griffith, D.W.T., Johnson, T.J., Reardon, J., Weise, D.R., 2011. Airborne and ground-based measurements of the trace gases and particles emitted by prescribed fires in the United States. Atmos. Chem. Phys. 11, 12197–12216.

Drinovec, L., Močnik, G., Zotter, P., Prévôt, A.S.H., Ruckstuhl, C., Coz, E., Rupakheti, M., Sciare, J., Müller, T., Wiedensohler, A., Hansen, A.D.A., 2015. The "dual-spot" Aethalometer: an improved measurement of aerosol black carbon with real-time loading compensation. Atmos. Meas. Tech. 8, 1965–1979. https://www.atmos-meas-tech.net/8/1965/2015/.

Forrister, H., Liu, J., Scheuer, E., et al., 2015. Evolution of brown carbon in wildfire plumes. Geophys. Res. Lett. 42 (11), 4623–4630. https://doi.org/10.1002/2015GL063897.

Freeborn, W., Chappell, L.M., Tobler, S., Kitchen, S.G., 2015. Monroe mountain aspen ecosystems restoration project fire ecology/fire/fuels specialist report. Richfield ranger District. Fishlake National Forest. https://www.fs.usda.gov/nfs/11558/www/nepa/91504_FSPLT3_2552273.pdf. Accessed December 9, 2020.

Friedli, H.R., Atlas, E., Stroud, V.R., Giovanni, L., Campos, T., Radke, L.F., 2001. Volatile organic trace gases emitted from North American wildfires. Global Biogeochem. Cycles 15, 435–452.

Gilman, J.B., Lerner, B.M., Kuster, W.C., Goldan, P.D., Warneke, C., Veres, P.R., Roberts, J.M., de Gouw, J.A., Burling, I.R., Yokelson, R.J., 2015. Biomass burning emissions and potential air quality impacts of volatile organic compounds and other trace gases from fuels common in the US. Atmos. Chem. Phys. 15, 13915–13938. https://www.atmos-chem-phys.net/15/13915/2015/.

Gullett, B., Aurell, J., Mitchell, W., Richardson, J., 2020. Use of an unmanned aircraft system to quantify NOx emissions from a natural gas boiler. Atmos. Meas. Technol. https://doi.org/10.5194/amt-2020-108 accepted for publication 15 December, 2020.

Hansen, A.D.A., 2005. The aethalometer. Magee scientific company. Berkeley, California, USA. https://www.psi.ch/sites/default/files/import/lac/ProjectAddonCatcosOperationsEN/Aethalometer_book_2005.07.02.pdf. Accessed April 29, 2020.

Hodshire, A.L., Akherati, A., Alvarado, M.J., Brown-Steiner, B., Jathar, S.H., Jimenez, J. L., Kreidenweis, S.M., Lonsdale, C.R., Onasch, T.B., Ortega, A.M., Pierce, J.R., 2019. Aging effects on biomass burning aerosol mass and composition: a critical review of field and laboratory studies. Environ. Sci. Technol. 53, 10007–10022. https://doi.org/10.1021/acs.est.9b02588.

Holder, A.L., Hagler, G.S.W., Aurell, J., Hays, M.D., Gullett, B.K., 2016. Particulate matter and black carbon optical properties and emission factors from prescribed fires in the southeastern United States. J. Geophys. Res. Atmos. 121, 3465–3483. https://doi.org/10.1002/2015JD024321.

Hsieh, Y.-P., Bugna, G., Robertson, K., 2018. Thermochemical properties of PM2.5 as indicator of combustion phase of fires. Atmosphere 9, 230.
Hyde, J., Yedinak, K., Talhelm, A., Smith, A., Bowman, D., Johnson, F., Lahm, P., Fitch, M., Tinkham, W., 2017. Air quality policy and fire management responses addressing smoke from wildland fires in the United States and Australia. Int. J. Wildland Fire 26, 347–363.
Jaffe, D.A., O'Neill, S.M., Larkin, N.K., Holder, A.L., Peterson, D.L., Halofsky, J.E., Rappold, A.G., 2020. Wildfire and prescribed burning impacts on air quality in the United States. J. Air Waste Manag. 70 (6), 583–615. https://doi.org/10.1080/10962247.2020.1749731.
Janssen, L.H.J.M., van Wakeren, J.H.A., van Duuren, H., Elshout, A.J., 1988. A classification of NO oxidation rates in power plant plumes based on atmospheric conditions. Atmos. Environ. 22, 43–53.
Jen, C.N., Hatch, L.E., Selimovic, V., Yokelson, R.J., Weber, R., Fernandez, A.E., Kreisberg, N.M., Barsanti, K.C., Goldstein, A.H., 2019. Speciated and total emission factors of particulate organics from burning western US wildland fuels and their dependence on combustion efficiency. Atmos. Chem. Phys. 19, 1013–1026. https://www.atmos-chem-phys.net/19/1013/2019/.
Khan, B., Hays, M.D., Geron, C., Jetter, J., 2012. Differences in the OC/EC ratios that characterize ambient and source aerosols due to thermal-optical analysis. Aerosol Sci. Technol. 46, 127–137.
Kim, Y.H., Warren, S.H., Krantz, Q.T., King, C., Jaskot, R., Preston, W.T., George, B.J., Hays, M.D., Landis, M.S., Higuchi, M., DeMarini, D.M., Gilmour, M.I., 2018. Mutagenicity and lung toxicity of smoldering vs. Flaming emissions from various biomass fuels: implications for health effects from wildland fires. Environ. Health Perspect. 126, 17011, 017011.
Krause, D.F., Leirvik, F., 2018. Field measurement of BC emissions from rolvsnes well test flare. SINTEF. https://sintef.brage.unit.no/sintef-xmlui/bitstream/handle/11250/2570241/OC2018%2BF-087%2BFlaring%2BReport.pdf?sequence=1&isAllowed=y. Accessed March 10, 2020.
Laursen, K.K., Hobbs, P.V., Radke, L.F., Rasmussen, R.A., 1992. Some trace gas emissions from North American biomass fires with an assessment of regional and global fluxes from biomass burning. J. Geophys. Res. Atmos. 97, 20687–20701. https://doi.org/10.1029/92JD02168.
Levin, E.J.T., McMeeking, G.R., Carrico, C.M., Mack, L.E., Kreidenweis, S.M., Wold, C.E., Moosmüller, H., Arnott, W.P., Hao, W.M., Collett Jr., J.L., Malm, W.C., 2010. Biomass burning smoke aerosol properties measured during Fire Laboratory at Missoula Experiments (FLAME). J. Geophys. Res. Atmos. 115. https://agupubs.onlinelibrary.wiley.com/doi/abs/10.1029/2009JD013601.
Li, H., Lamb, K.D., Schwarz, J.P., Selimovic, V., Yokelson, R.J., McMeeking, G.R., May, A. A., 2019. Inter-comparison of black carbon measurement methods for simulated open biomass burning emissions. Atmos. Environ. 206, 156–169. http://www.sciencedirect.com/science/article/pii/S1352231019301724.
Liu, X., Huey, L., Yokelson, R., Selimovic, V., Simpson, I., Müller, M., Jimenez, J., Campuzano-Jost, P., Beyersdorf, A., Blake, D., Butterfield, Z., Choi, Y., Crounse, J., Day, D., Diskin, G., Dubey, M., Fortner, E., Hanisco, T., Hu, W., Wolfe, G., 2017. Airborne measurements of western U.S. wildfire emissions: comparison with prescribed burning and air quality implications: western U.S. Wildfire Emissions. J. Geophys. Res. Atmos. 122.
Liu, Y., Kochanski, A., Baker, K.R., Mell, W., Linn, R., Paugam, R., Mandel, J., Fournier, A., Jenkins, M.A., Goodrick, S., Achtemeier, G., Zhao, F., Ottmar, R., French, N.H.F., Larkin, N., Brown, T., Hudak, A., Dickinson, M., Potter, B., Clements, C., Urbanski, S., Prichard, S., Watts, A., McNamara, D., 2019. Fire behaviour and smoke modelling: model improvement and measurement needs for next-generation smoke research and forecasting systems. Int. J. Wildland Fire 28, 570–588. https://doi.org/10.1071/WF18204.
Mladenovic, M., Dakic, D., Nemoda, S., Paprika, M., Komatina, M., Repic, B., Eric, A., 2016. The combustion of biomass - the impact of its types and combustion technologies on the emission of nitrogen oxide. Hem. Ind. 70, 287–298.
Nelson, K., Boehmler, J., Khlystov, A., Moosmuller, H., Samburova, V., Bhattarai, C., Wilcox, E., Watts, A., 2019. A multipollutant smoke emissions sensing and sampling instrument package for unmanned aircraft systems: development and testing. Fire 2, 32.
NIOSH Method 5040, 1999. Elemental carbon (diesel particulate). Issue 3. NIOSH Manual of Analytical Methods, 30 September, fourth ed.
Ottmar, R.D.U.S., 2013. Forest Service Pacific Northwest Research Station. CONSUME fuel consumption and emissions software. https://www.fs.usda.gov/pnw/projects/consume-fuel-consumption-and-emissions-software. (Accessed 9 December 2020).
Ottmar, R., Brown, T., French, N., Larkin, N., 2017. Fire and smoke model evaluation experiment (FASMEE) study plan. Joint fire science program, boise, Idaho. https://www.firescience.gov/documents/2017_JFSP_ProgressReport.pdf. Accessed March 10, 2020.
Prichard, S., Larkin, N., Ottmar, R., French, N., Baker, K., Brown, T., Clements, C., Dickinson, M., Hudak, A., Kochanski, A., Linn, R., Liu, Y., Potter, B., Mell, W., Tanzer, D., Urbanski, S., Watts, A., 2019. The fire and smoke model evaluation experiment—a plan for integrated, large fire–atmosphere field campaigns. Atmosphere 10, 66.
Prichard, S.J., O'Neill, S.M., Eagle, P., Andreu, A.G., Drye, B., Dubowy, J., Urbanski, S., Strand, T.M., 2020. Wildland fire emission factors in North America: synthesis of existing data, measurement needs and management applications. Int. J. Wildland Fire 29, 132–147. https://doi.org/10.1071/WF19066.
Radke, L.F., Hegg, D.A., Hobbs, P.V., Nance, J.D., Lyons, J.H., Laursen, K.K., Weiss, R.E., Riggan, P.J., Ward, D.E., 1991. Particulate and Trace Gas Emissions from Large Biomass Fires in North America. Massachusetts Inst of Tech Press, United States.
Rappold, A.G., Reyes, J., Pouliot, G., Cascio, W.E., Diaz-Sanchez, D., 2017. Community vulnerability to health impacts of wildland fire smoke exposure. Environ. Sci. Technol. 51, 6674–6682. https://doi.org/10.1021/acs.est.6b06200.
Selimovic, V., Yokelson, R.J., Warneke, C., Roberts, J.M., de Gouw, J., Reardon, J., Griffith, D.W.T., 2018. Aerosol optical properties and trace gas emissions by PAX and OP-FTIR for laboratory-simulated western US wildfires during FIREX. Atmos. Chem. Phys. 18, 2929–2948. https://www.atmos-chem-phys.net/18/2929/2018/.
Simpson, I.J., Akagi, S.K., Barletta, B., Blake, N.J., Choi, Y., Diskin, G.S., Fried, A., Fuelberg, H.E., Meinardi, S., Rowland, F.S., Vay, S.A., Weinheimer, A.J., Wennberg, P.O., Wiebring, P., Wisthaler, A., Yang, M., Yokelson, R.J., Blake, D.R., 2011. Boreal forest fire emissions in fresh Canadian smoke plumes: C-1-C-10 volatile organic compounds (VOCs), CO_2, CO, NO_2, NO, HCN and CH_3CN. Atmos. Chem. Phys. 11, 6445–6463. https://www.atmos-chem-phys.net/11/6445/2011/.
Subramanian, R., Khlystov, A.Y., Cabada, J.C., Robinson, A.L., 2004. Positive and negative artifacts in particulate organic carbon measurements with denuded and undenuded sampler configurations special issue of aerosol science and technology on findings from the fine particulate matter supersites program. Aerosol Sci. Technol. 38, 27–48. https://doi.org/10.1080/02786820390229354.
Thomas, S.C., Martin, A.R., 2012. Carbon content of tree tissues: a synthesis. Forests 3, 332–352.
Urbanski, S.P., 2013. Combustion efficiency and emission factors for wildfire-season fires in mixed conifer forests of the northern Rocky Mountains, US. Atmos. Chem. Phys. 13, 7241–7262.
U.S. EPA, 2013. Photochemical assessment monitoring stations compound target list. https://www3.epa.gov/ttnamti1/files/ambient/pams/targetlist.pdf. Accessed June 9 2017.
U.S. EPA Compendium Method IO-3.3, 1999. Determination of metals in ambient particulate matter using X-Ray Fluorescence (XRF) Spectroscopy. http://www.epa.gov/ttnamti1/files/ambient/inorganic/mthd-3-3.pdf. Accessed February 13, 2019.
U.S. EPA Compendium Method TO-11A, 1999. Determination of formaldehyde in ambient air using adsorbent cartridge followed by high performance liquid chromatography (HPLC). https://www3.epa.gov/ttnamti1/files/ambient/airtox/to-11ar.pdf. Accessed July 25, 2016.
U.S. EPA Hazardous Air Pollution List, 2008. Clean air act: title 42 - the public health and welfare. U.S. Government printing Office. http://www.gpo.gov/fdsys/pkg/USCODE-2008-title42/pdf/USCODE-2008-title42-chap85.pdf. Accessed October 16 2019.
U.S. EPA Method TO-17, 1997. Determination of volatile organic compounds in ambient air using active sampling onto sorbent tubes. http://www.epa.gov/ttnamti1/files/ambient/airtox/to-17r.pdf. Accessed July 25, 2013.
U.S. Forest Service, 2019. South Monroe mountain aspen prescribed fire. https://www.fs.usda.gov/Internet/FSE_DOCUMENTS/fseprd561561.pdf. Accessed April 7, 2020.
USDA, Forest Service, 2015. Final environmental impact statement, appendices J-R, Monroe mountain aspen ecosystems restoration project, Richfield ranger District, Fishlake national forest, sevier and piute counties. Utah, Accessed March 10, 2020. https://www.fs.usda.gov/nfs/11558/www/nepa/91504_FSPLT3_2552275.pdf.
Vasileva, A., Moiseenko, K., Skorokhod, A., Belikov, I., Kopeikin, V., Lavrova, O., 2017. Emission ratios of trace gases and particles for Siberian forest fires on the basis of mobile ground observations. Atmos. Chem. Phys. 17, 12303–12325. https://www.atmos-chem-phys.net/17/12303/2017/.
Volkova, L., Meyer, C.P.M., Murphy, S., Fairman, T., Reisen, F., Weston, C., 2014. Fuel reduction burning mitigates wildfire effects on forest carbon and greenhouse gas emission. Int. J. Wildland Fire 23, 771–780. https://doi.org/10.1071/WF14009.
Ward, D.E., Hao, W.M., 1991. Projections of emissions from burning of biomass foruse in studies of global climate and atmospheric chemistry. In: Air & Waste Management Association **June** 16–21, pp. 91–128. https://www.fs.fed.us/rm/pubs_journals/1991/rmrs_1991_ward_d001.pdf.
Ward, D.E., Hardy, C.C., 1988. Organic and elemental profiles for smoke from prescribed fires. Int. Spec. Conf. of the J Air Waste Manag. 299–321.
Ward, D.E., Radke, L.F., 1993. Emissions measurements from vegetation fires: a comparative evaluation of methods and results. In: Crutzen, P.J., Goldammer, J.G. (Eds.), Environmental Sciences Research Report; Fire in the Environment: the Ecological, Atmospheric, and Climatic Importance of Vegetation Fires, pp. 53–76.
Ward, D.E., Nelson, R.M., Adams, D.F., 1979. Forest fire smoke plume documentation. In: Proceedings of the Seventy-Seventh Annual Meeting of the Air Pollution Control Association Pap, 079-6.3.
Weise, D., Johnson, T., Reardon, J., 2015. Particulate and trace gas emissions from prescribed burns in southeastern U.S. fuel types: summary of a 5-year project. Fire Saf. J. 74, 71–81.
Williams, C.L., Emerson, R.M., Tumuluru, J.S., 2017. Biomass compositional analysis for conversion to renewable fuels and chemicals. Biomass Volume Estimation and Valorization for Energy 251–270. https://doi.org/10.5772/65777. IntechOpen.
Yokelson, R.J., Burling, I.R., Gilman, J.B., Warneke, C., Stockwell, C.E., de Gouw, J., Akagi, S.K., Urbanski, S.P., Veres, P., Roberts, J.M., Kuster, W.C., Reardon, J., Griffith, D.W.T., Johnson, T.J., Hosseini, S., Miller, J.W., Cocker Iii, D.R., Jung, H., Weise, D.R., 2013. Coupling field and laboratory measurements to estimate the emission factors of identified and unidentified trace gases for prescribed fires. Atmos. Chem. Phys. 13, 89–116. https://doi.org/10.5194/acp-13-89-2013.
Zhou, X., Aurell, J., Mitchell, W., Tabor, D., Gullett, B., 2017. A small, lightweight multipollutant sensor system for ground-mobile and aerial emission sampling from open area sources. Atmos. Environ. 154, 31–41.